# Macroscopic-Microscopic Fission Yields

*Matthew* Mumpower[1,2,*], *Trevor* Sprouse[1], *Marc* Verriere[3], *Nicole* Vassh[4], and *Jorgen* Randrup[5]

[1]Theoretical Division, Los Alamos National Laboratory, Los Alamos, NM 87545, USA
[2]Center for Theoretical Astrophysics, Los Alamos National Laboratory, Los Alamos, NM 87545, USA
[3]Nuclear and Data Theory Group, Nuclear and Chemical Science Division, Lawrence Livermore National Laboratory, Livermore, CA 94550, USA
[4]TRIUMF, 4004 Wesbrook Mall, Vancouver, British Columbia V6T 2A3, Canada
[5]Nuclear Science Division, Lawrence Berkeley National Laboratory, Berkeley, CA 94720, USA

**Abstract.** We utilize the macroscopic-microscopic approach to fission to calculate nascent fragment distributions. Assuming strongly damped shape motion, we run many iterations of a Metropolis random walk across nuclear potential-energy surfaces to obtain sufficient scission statistics. Our nuclear potential surfaces consist of a macroscopic energy from the Finite-Range Liquid-Drop Model (FRLDM) and microscopic terms that arise from the single-particle spectra. We compare our predictions for two major actinides to experimental data. We present global trends from this modeling that manifest as a function of mass number of the fissioning species. We discuss the impact of fission yield modeling on nucleosynthetic outcomes.

## 1 Introduction

The description of nuclear fission remains a challenge to present day theoretical modeling [1]. A quantum system that undergoes fission initially starts in a compact shape configuration that progresses to more elongated shapes before terminating with scission, when two (or more) fragments become physically separated. The challenge of describing this process is further compounded by the dearth of experimental measurements presently available [2].

Microscopic models describe the fission process from the minimization of an energy density functional assuming a system of independent nucleons. The space is subject to constraints on the density distribution of nucleons which governs overall distortion (Q2), or on higher multipole moments like the octupole moment (Q3) which influences reflection asymmetry of the system [3]. Present computational bottlenecks limit the application of these models to a select few nuclei, but progress is being made to overcome these obstacles, for instance by using Machine Learning based emulators [4].

Macroscopic-microscopic models in contrast are computationally efficient [5]. These models offer the ability to describe larger multidimensional shape spaces that are requisite for the generation of potential energy surfaces used in the computation of fission yields [6]. One of the leading models in this approach has been the Finite-Range Liquid-Drop Model (FRLDM), which has shown excellent performance when predicting fission yields for a wide variety of nuclei [7, 8]. The potential energy surfaces of this model can also be used to calculate fission barriers which are important in determining the propensity of a particular nucleus in undergoing fission [9]. More recently, improvements have been made to this model to use more quantum mechanical level densities and to predict total kinetic energies necessary for the de-excitation of the nascent products [10–15].

Nuclear fission ties directly into the synthesis of the heaviest elements in nature, thought to occur in rare astrophysical environments. [16]. As the astrophysical rapid neutron capture process (*r*-process) of nucleosynthesis is believed to be responsible for all of the actinide production in nature, it is likely that some fission will have occurred during the production of these elements. The extent of nuclear fission and resultant impact in the *r*-process remains an open question [17, 18]. Neutron-induced [19], $\beta$-delayed [20–22], and spontaneous [23, 24] fission may all contribute depending on the conditions present in the explosive environment.

Figure 1 shows the broad impact that fission can have across the chart of nuclides. Fission operates, and has the capacity to terminate nucleosynthesis in the upper right portion of the diagram (teal). Depending on the species (or set of species) that undergo fission in the *r*-process, the fission products may be distributed over a wide range in mass number (purple). Much of this spread is outside known data (orange) where only a few relevant nuclear properties may be measured. Stable nuclei are shown by black squares for reference.

In this conference proceedings we review work performed over the past half decade on the calculation of fission fragment yields using the FRLDM macroscopic-microscopic model. We discuss trends arising from our calculations and the implications of these calculations on

*e-mail: mumpower@lanl.gov

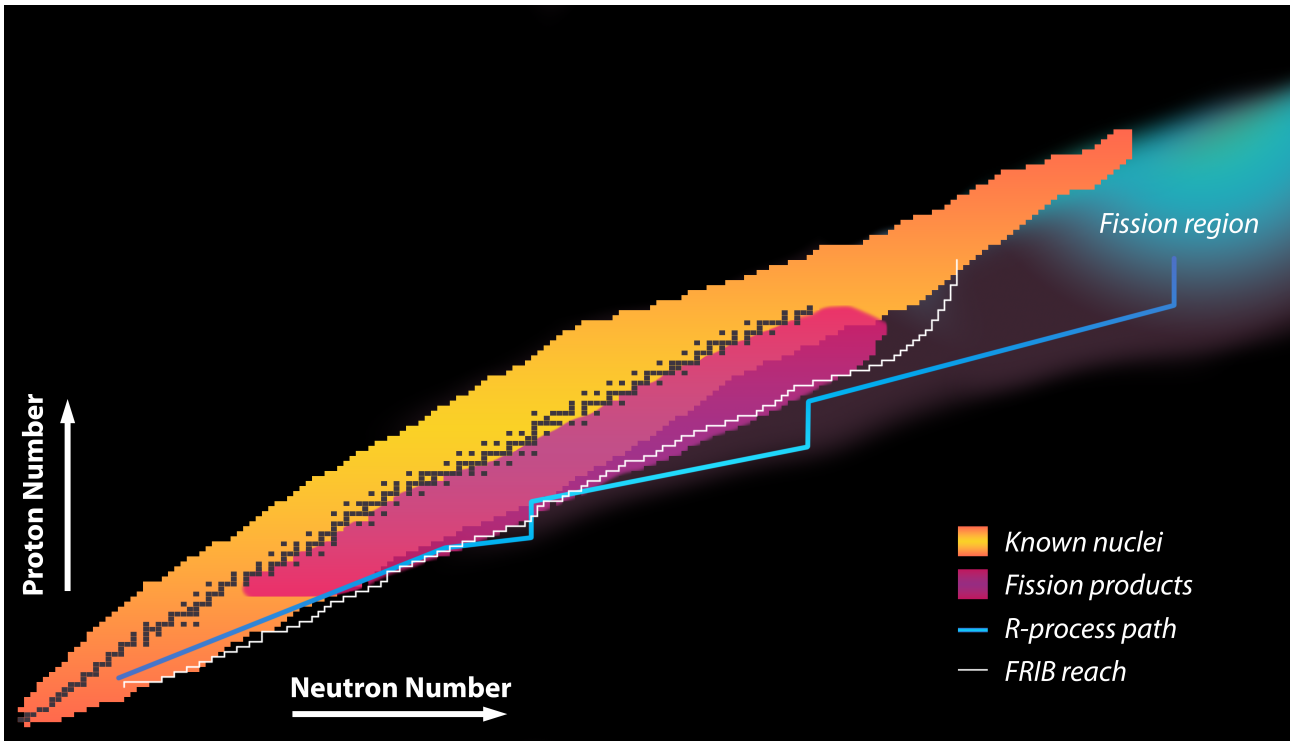


**Figure 1.** The chart of nuclides indicating where fission operates (teal) and deposits its products (purple). Stable nuclei (black squares), nuclei with measurements (orange), a schematic path along the neutron dripline of the *r*-process (blue line) and the possible maximum extent of FRIB are shown for reference.

the formation of the heavy elements during *r*-process nucleosynthesis.

## 2 Macroscopic-microscopic yields

The calculation of fission yields in our approach assumes the dynamics is akin to Brownian shape motion using five shape degrees of freedom [25]. This is simulated numerically by a random walk across the nuclear potential energy surface [26]. The random walks continue until reaching a specified critical neck radius between the two fragments. The value of 2.5 fm has been found to be a good stopping point where the mass partition between the two fragments is frozen in [7]. By accumulating statistics of scission events, the fragment yield may be built up trajectory by trajectory. An overview of these calculations along with testing of various assumptions is provided in Ref. [27].

It is instructive to analyze the distributions of scission configurations in the five shape degrees of freedom. Here we use integer grids for the representation of these quantities. The degrees of freedom are the overall quadrupole moment (represented by integer, $I$), the neck radius ($J$), left fragment deformation ($K$), right fragment deformation ($L$), and mass asymmetry ($M$). Figure 2 shows the scission distributions for each of the five coordinates respectively. The nucleus under consideration is $^{236}$U at an incident energy above its fission barrier (~ 6 MeV). The mass quadrupole is spread over ten integer units representing a large spread in overall elongation at scission; this distribution is almost Gaussian in nature. The neck radius distribution is much more narrow, owing to the sharp cut we impose at 2.5 fm. The widest distributions are found in the deformation parameters of the left and right fragments, indicating a large spread in the shapes of the final nascent fragments. The mass asymmetry distribution is offset from zero, implying an asymmetric yield for this nucleus at the given incident energy.

An example of our fission yield calculations versus data (black circles) is shown for $^{236}$U and $^{240}$Pu in Figure 3. The initial excitation energy for $^{236}$U is above the fission barrier, around 6 MeV. The initial excitation energy for $^{240}$Pu is at 20 MeV. The data for $^{236}$U comes from Ref. [28]. The data for $^{240}$Pu comes from Ref. [29].

To obtain the spread in the mass yields, we calculate the fission transport via two different procedures. The first method is via Brownian shape motion on a discrete lattice, as in the results of Fig. 2. The second method performs the same random walk except on a continuous grid. This method results in close agreement with the discrete case giving reassurance with our choice of discrete grid. The third method implements fission transport via the Smoluchowski equations for fission [26]. The fission transport in this case relies on the calculation of a mobility tensor instead of on the gradient of the potential energy surface alone (as in the Brownian case).

We compile the same statistics in each of these three cases taking the maximum and minimum values for $Y(A)$ to define the spread. This procedure provides an estimate of the error bar stemming from the uncertainty in transport physics. We find an overall small spread in these distribu-

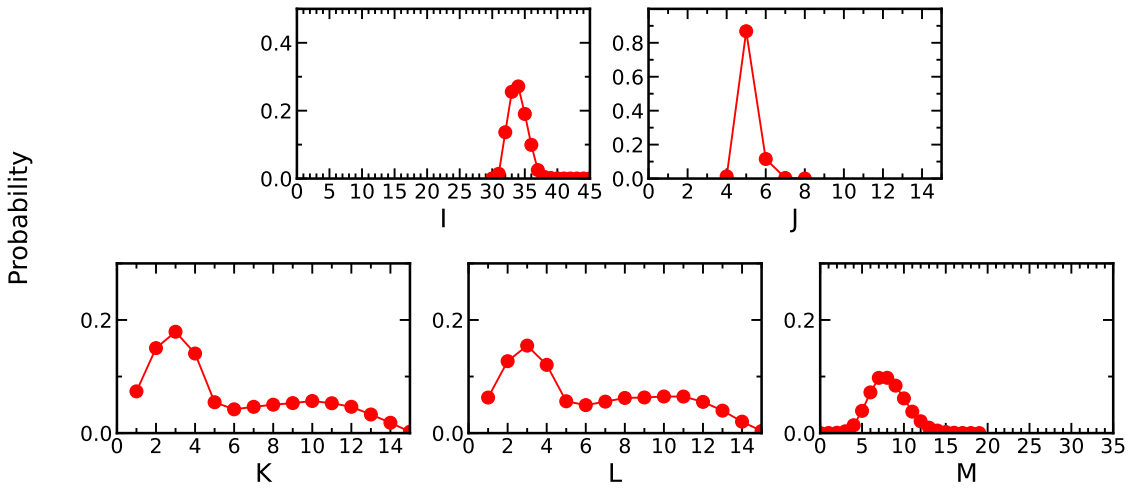


**Figure 2.** Probabilities to land in each of the five shape degrees of freedom when calculating the fission yield of $^{236}$U at an incident energy just above the fission barrier. Probabilities are scaled to sum to unity in each panel.

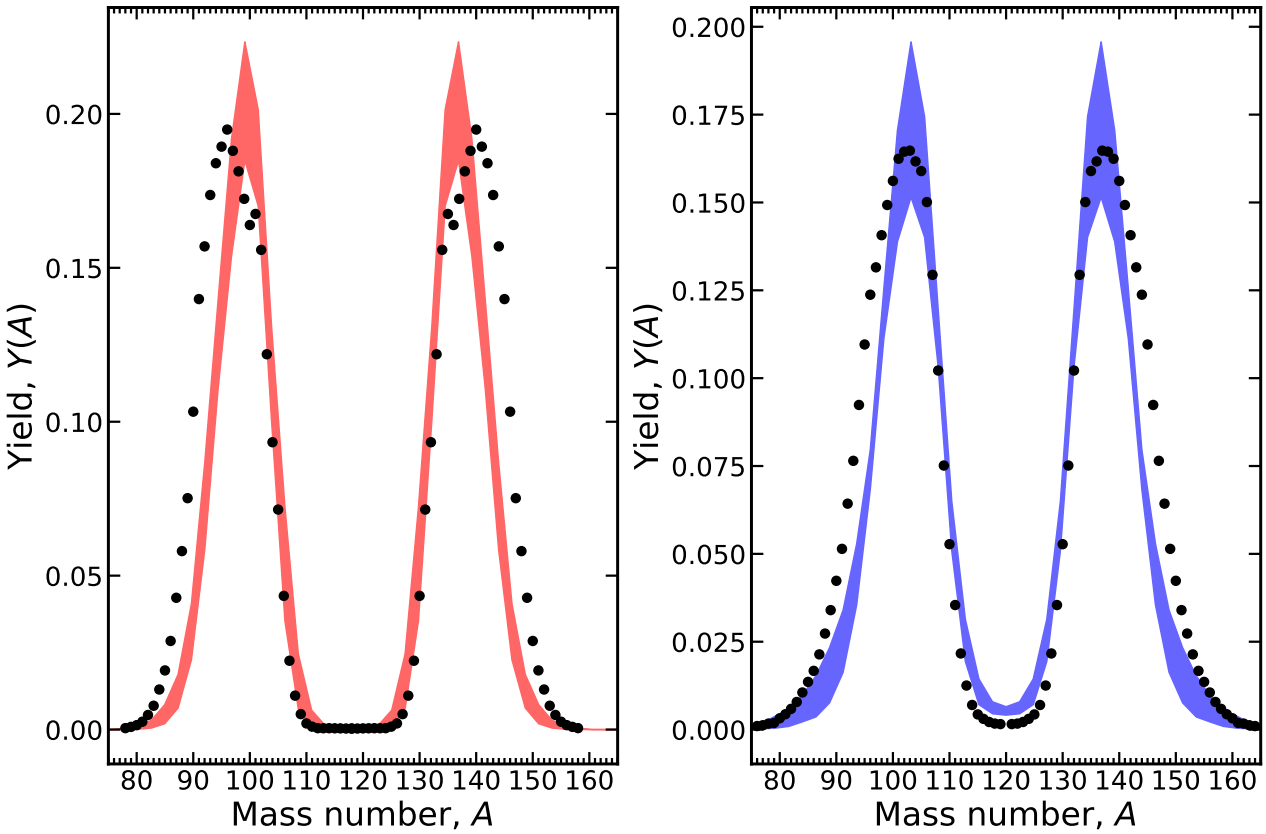


**Figure 3.** Mass yields, $Y(A)$, for $^{236}$U (left) and $^{240}$Pu (right) for a variation of fission transport assumptions. Data shown by black circles in the left [28] and right [29] panels respectively. The scale of the yields is arbitrary.

tions and note that no major shifts, beyond 3 mass units, in the peaks of the distribution are found. These error estimates are on the order of present day uncertainties in experimentally measured mass yields. Highly accurate and precise experimental data may one day be able to constrain the different models of fission transport.

We have extended the Brownian transport of mass yields well beyond the major actinides. Fission yields have been computed for all species relevant to the astrophysical *r*-process using FRLDM in Ref. [27]. In this work it was found that the yields have a contrasting behavior across the chart of nuclides. As has been shown above, actinides near the stable isotopes are found to split asymmetrically. Increasing proton numbers beyond the actinides tend to split more symmetrically. When neutrons are added to these systems, the mass yield is found to widen. This is a general trend as one pushes into the region of unknown superheavy nuclei. For *r*-process nuclei $\sim 40$ or more neutrons from stable nuclei, the yields are found to be more than double the width of a prototypical actinide. In this case it does not make sense to distinguish between asymmetric and symmetric splitting as the fragments are distributed over a wide mass range. Consequences of this observation are discussed in the next section.

To visualize these trends, we plot in Figure 4 the width, $W_d$, and asymmetry factor, $S_f$, as a function of mass number. The width is calculated as the number of fragment masses with a yield above 1% as in Ref. [27]. This value is averaged for every fission species (with the same mass number) to produce the dashed purple line. The standard deviation of this distribution is shown by the shaded region. Similarly, the asymmetry factor, $S_f$, is calculated as the difference in fragment mass number between the maximum yield of the distribution and the symmetric split value, $A_0/2$, as in Ref. [27]. The average and standard deviation of this distribution is calculated in like manner as above, for fixed mass number of the fissioning system.

Several interesting trends can be found in this figure. First, it is clear that the width of the mass distributions tend to increase with increasing mass number of the fissioning system. Major actinide nuclei typically have $W_d \lesssim 45$ while a heavy *r*-process nucleus undergoing fission, may have a width $W_d \gtrsim 80$. The asymmetry factor also has distinct behavior as a function of mass number. Virtually all nuclei below mass number of $A \sim 200$ are found to fission asymmetrically while there is a strong region of symmetric splits around mass number $A \sim 220$. In general a heavy *r*-process nucleus is most likely to fission asymmetrically, however, we do note that there is a larger spread in this distribution as compared with the spread in mass yield widths.

Another important aspect of fission yield calculations in the context of nucleosynthesis is the energy released as nuclei undergo fission. The fission $Q$ value represents the energy released during the fission process. An estimate for the fission $Q$ value may calculated from our yields via the relation,

$$Q_f \sim M(Z_0, A_0) - \sum_{Z,A} Y(Z,A) M(Z,A) \qquad (1)$$

where the first term is the mass of the fissioning nucleus, and the second terms consist of the fragment yield, $Y(Z,A)$, and fragment mass, $M(Z,A)$, of the fission product. Different fission mechanisms (neutron-induced, $\beta$-delayed, or spontaneous) will slightly modify Equation 1 depending on the participating reactants in the reaction process.

We use the FRDM2012 for the prediction of masses [30]. The trend in fission $Q$ values is most apparent when plotting versus proton number of the fissioning species. We plot the mean value of $Q_f$ and its standard deviation (blue bars) along an isotopic chain as a function of proton number in Figure 5. The small spread of our calculations shows that there is minimal difference in fission $Q$-value along a given isotopic chain. The functional form of the $Q_f$ versus $Z_0$ relationship is well approximated by a quadratic form (red curve), $Q_f \approx aZ_0^2 + bZ_0 + c$. The formula is valid for $80 \leq Z_0 \leq 130$ and the coefficients of this fit are $a = 0.0414$, $b = -2.667$ and $c = 74.974$.

## 3 Impact of fission yields in nucleosynthesis

Pronounced fission impact during nucleosynthesis can occur via large deposition of material down to lighter mass regions as well as with a continual reprocessing of material, down, up and recycled again through the chart of nuclides. One of the consequences of significant fission during the synthesis of the heavy elements is the correlation between nuclei in the fission product region (recall Fig. 1). When this occurs, co-production of light and heavy fission products will ensue [31].

As an example of this phenomenon we simulate *r*-process nucleosynthesis in the dynamical ejecta of a neutron star merger using the Portable Routines for Integrated nucleoSynthesis Modeling (PRISM) reaction network [32]. The trajectory comes from the work of Ref. [33]. Figure 6 highlights a snapshot of the simulation at roughly 6 seconds. In the bottom panel, we find an *r*-process with robust fission deposition in the product region. Practically every nucleus populated between mass number $A \sim 80$ and $A \sim 190$ has been synthesized directly from fission products. The details of this conclusion is discussed in the nucleosynthesis tracing work of Sprouse *et al.* [32]. When summing abundances by mass number as shown in the upper panel a relatively flat trend is found between $A \sim 80$ and $A \sim 190$. The only deviation in this trend comes from the existence of the closed shell at neutron number $N = 82$.

Astronomical observations give some clues that fission may be operating in extreme environments that support the main component of the *r*-process. A particular example is the ratio of $^{129}$I to $^{247}$Cm in meteorites, which is directly connected to the conditions of the astrophysical site that produced them [34]. These two long-lived radioactive isotopes have similar half-lives (~15.6 Myr) despite being separated by nearly 120 mass units. This observational evidence constraints the last *r*-process event that polluted the pre-solar nebula.

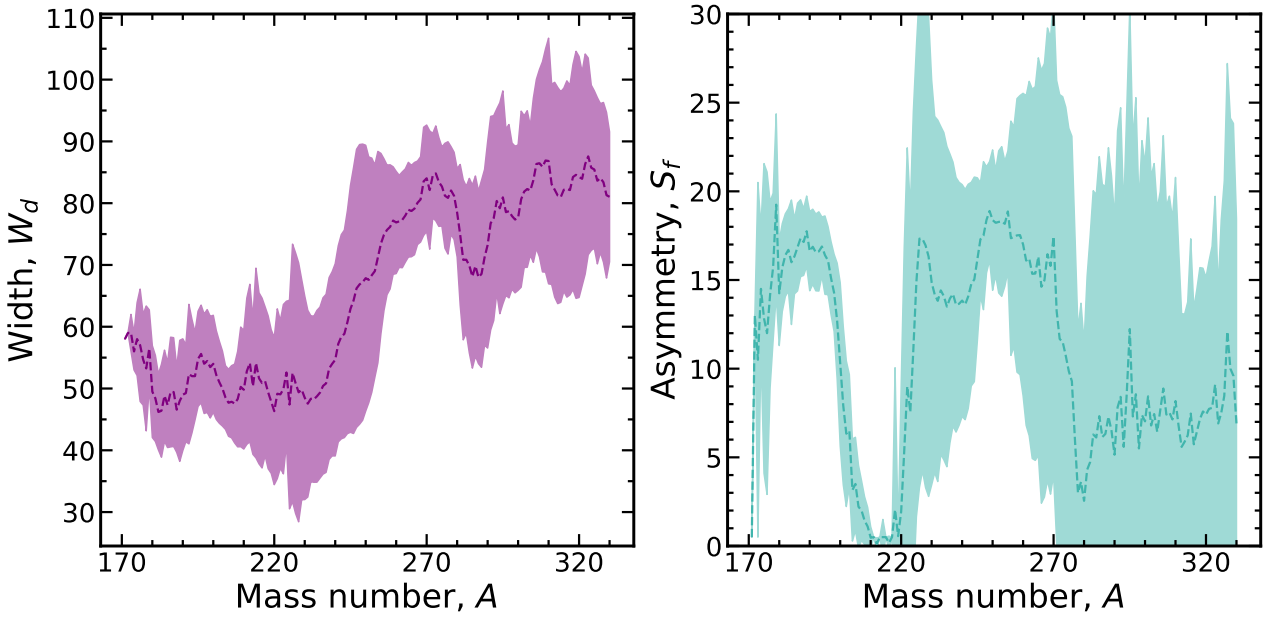


**Figure 4.** Trends found in the mass yields as a function of mass number of the fissioning species.

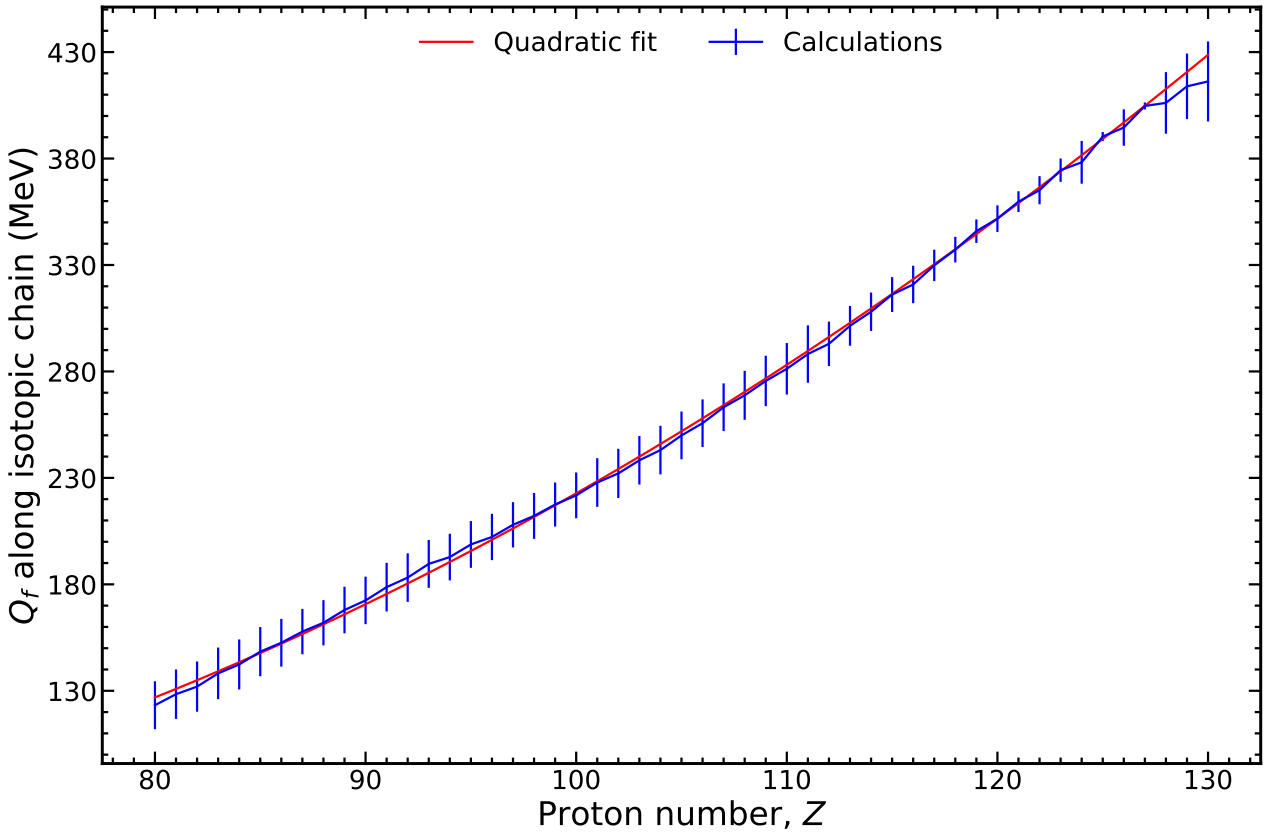


**Figure 5.** Trend in the average fission $Q$ value as a function of proton number. The trend is well approximated with a quadratic form in proton number, see text for fit details.

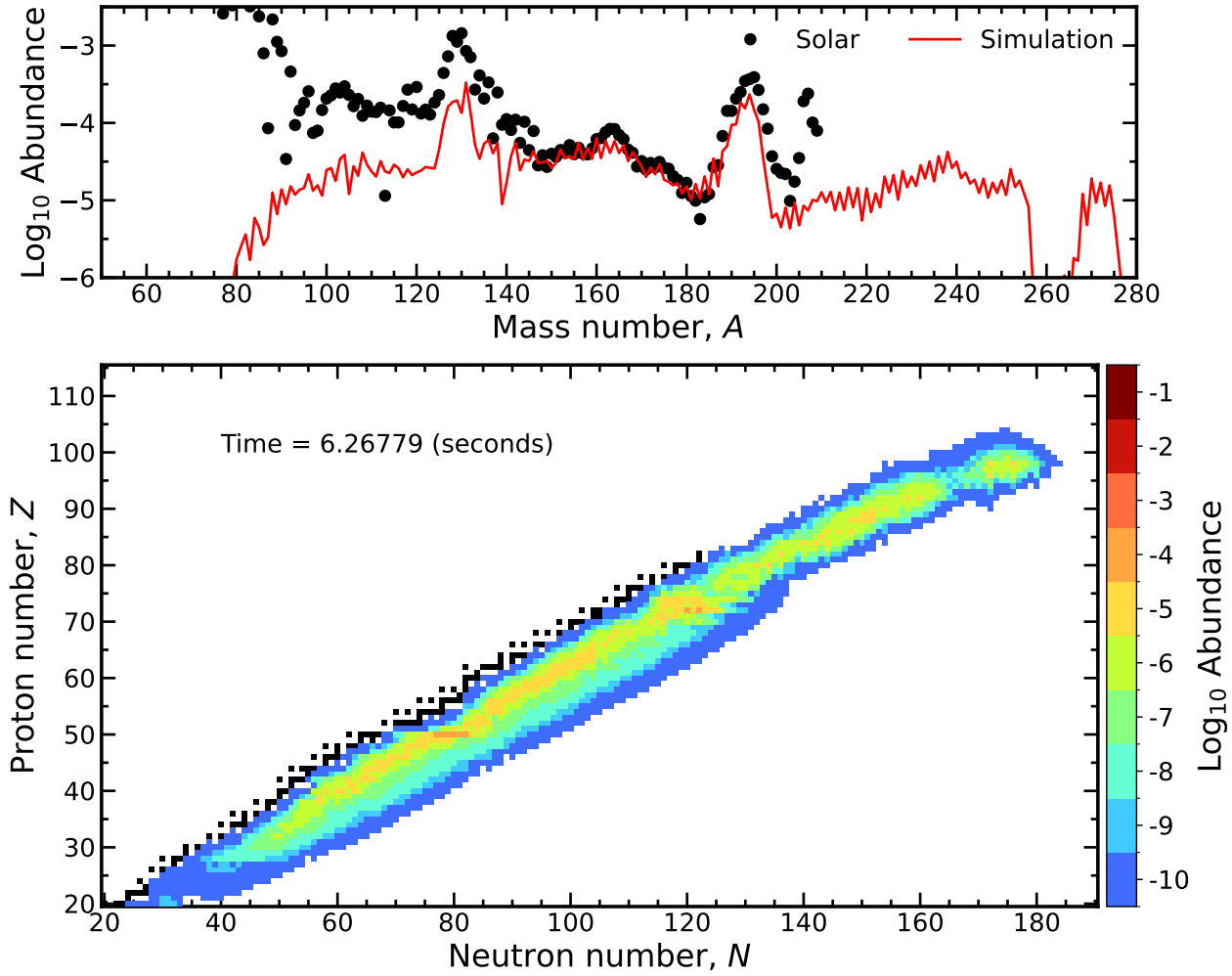


**Figure 6.** Simulation of *r*-process nucleosynthesis using a trajectory from the dynamical ejecta of a neutron star merger. Nuclear fission spreads out the abundances over a wide range of nuclei.

Separate evidence comes from a recent analysis of 42 metal-poor halo stars in the galaxy that hints at a correlation between light precious metals and lanthanides [35]. By deconvoluting different *r*-process contributions with a local scaling of elements, Roederer and colleagues were able to reproduce the trend of the co-production theory proposed by Vassh *et al.* [31]. The present database of metal-poor halo stars seems to confirm the presence of fission. Additional data on specific elements and the addition of presently unobserved stars will help to resolve whether this trend continues, or whether there are deviations. The exception to the trend, if found, will provide the most valuable constraint information regarding possible sites of the *r*-process.

Fission yields in the *r*-process also influence one other critical area that has future observational consequences. Nascent fission fragments can produce an enormous amount of $\gamma$-rays that span a wide range of energies as they de-excite. Precisely which nuclei emit $\gamma$-rays is dependent on how the fission fragments are distributed, in other words, on the prediction of fission yields. It has been established that $\gamma$-rays from freshly synthesized heavy nuclei offers a unique multi-messenger signal of astrophysical transients [36] and it was recently shown that distinct signals, like the 2.6 MeV line from the decay of $^{208}$Tl can be used as a proxy for actinide production [37]. Fission in particular provides a unique signature because of the very high energies ($\gtrsim$ 3 MeV) associated with the decay of the products on relatively long timescales after the rapid capture of neutrons has completed [38]. This signal is estimated to be observable within the galaxy and offers a unique follow up opportunity if a nearby event is ever recorded.

## 4 Concluding remarks

Many open questions remain regarding the prediction of fission yields of actinides and heavier nuclei. From the details of nuclear structure and reaction physics, to the behavior of superheavy nuclei in astrophysical environments, the study of nuclear fission offers many opportunities to continue to reveal the peculiarities of the strong interaction and improve our understanding of the origin of the heaviest elements. Macroscopic-microscopic model-

ing has been essential for advancing these endeavors and will continue to remain relevant as long as a concerted effort in the development and exploration of these models is sustained.

## 5 Acknowledgements

This work was supported by the Advanced Scientific Computing program and through the Laboratory Directed Research and Development program under project number 20230052ER at LANL. LANL is operated by Triad National Security, LLC, for the National Nuclear Security Administration of U.S. Department of Energy (Contract No. 89233218CNA000001). This work is released under LA-UR-24-22780.

## References

[1] M. Bender, R. Bernard, G. Bertsch, S. Chiba, J. Dobaczewski, N. Dubray, S.A. Giuliani, K. Hagino, D. Lacroix, Z. Li et al., Journal of Physics G: Nuclear and Particle Physics **47**, 113002 (2020)

[2] K.H. Schmidt, B. Jurado, Reports on Progress in Physics **81**, 106301 (2018)

[3] N. Schunck, L.M. Robledo, Reports on Progress in Physics **79**, 116301 (2016)

[4] M. Verriere, N. Schunck, I. Kim, P. Marević, K. Quinlan, M.N. Ngo, D. Regnier, R.D. Lasseri, Frontiers in Physics **10** (2022)

[5] C. Ishizuka, X. Zhang, K. Shimada, M. Usang, F. Ivanyuk, S. Chiba, Frontiers in Physics **11** (2023)

[6] F.A. Ivanyuk, C. Ishizuka, S. Chiba, Phys. Rev. C **109**, 034602 (2024)

[7] J. Randrup, P. Möller, Phys. Rev. C**88**, 064606 (2013)

[8] P. Möller, J. Randrup, Phys. Rev. C**91**, 044316 (2015)

[9] P. Möller, A.J. Sierk, T. Ichikawa, A. Iwamoto, M. Mumpower, Phys. Rev. C**91**, 024310 (2015)

[10] M. Albertsson, B.G. Carlsson, T. Døssing, P. Möller, J. Randrup, S. Åberg, European Physical Journal A **56**, 46 (2020)

[11] M. Albertsson, B.G. Carlsson, T. Døssing, P. Möller, J. Randrup, S. Åberg, Physics Letters B **803**, 135276 (2020)

[12] A.E. Lovell, T. Kawano, S. Okumura, I. Stetcu, M.R. Mumpower, P. Talou, Phys. Rev. C**103**, 014615 (2021)

[13] M. Albertsson, B.G. Carlsson, T. Døssing, P. Möller, J. Randrup, S. Åberg, Phys. Rev. C**103**, 014609 (2021)

[14] M. Albertsson, B.G. Carlsson, T. Døssing, P. Möller, J. Randrup, S. Åberg, Phys. Rev. C**104**, 064616 (2021)

[15] S. Åberg, M. Albertsson, B. Carlsson, T. Døssing, P. Möller, J. Randrup, *Nuclear Structure Effects in Fission*, in *Journal of Physics Conference Series* (2023), Vol. 2586 of *Journal of Physics Conference Series*, p. 012027

[16] E.M. Holmbeck, T.M. Sprouse, M.R. Mumpower, European Physical Journal A **59**, 28 (2023)

[17] T.M. Sprouse, M.R. Mumpower, R. Surman, *Following Fission Products in Explosive Astrophysical Environments*, in *European Physical Journal Web of Conferences* (2020), Vol. 242 of *European Physical Journal Web of Conferences*, p. 04001

[18] N. Vassh, M. Mumpower, T. Sprouse, R. Surman, R. Vogt, *Probing the fission properties of neutron-rich actinides with the astrophysical r process*, in *European Physical Journal Web of Conferences* (2020), Vol. 242 of *European Physical Journal Web of Conferences*, p. 04002

[19] G. Martínez-Pinedo, D. Mocelj, N. Zinner, A. Kelić, K. Langanke, I. Panov, B. Pfeiffer, T. Rauscher, K.H. Schmidt, F.K. Thielemann, Progress in Particle and Nuclear Physics **59**, 199 (2007), international Workshop on Nuclear Physics 28th Course

[20] M.R. Mumpower, T. Kawano, T.M. Sprouse, N. Vassh, E.M. Holmbeck, R. Surman, P. Möller, ApJ**869**, 14 (2018)

[21] F. Minato, T. Marketin, N. Paar, Phys. Rev. C **104**, 044321 (2021)

[22] M.R. Mumpower, T. Kawano, T.M. Sprouse, Phys. Rev. C**106**, 065805 (2022)

[23] S.A. Giuliani, G. Martínez-Pinedo, M.R. Wu, L.M. Robledo, Physical Review C **102** (2020)

[24] Y.W. Hao, Y.F. Niu, Z.M. Niu, The Astrophysical Journal **933**, 3 (2022)

[25] J. Randrup, P. Möller, Phys. Rev. Lett.**106**, 132503 (2011)

[26] J. Randrup, P. Möller, A.J. Sierk, Phys. Rev. C**84**, 034613 (2011)

[27] M.R. Mumpower, P. Jaffke, M. Verriere, J. Randrup, Phys. Rev. C**101**, 054607 (2020)

[28] C. Straede, C. Budtz-Jørgensen, H.H. Knitter, Nuclear Physics A **462**, 85 (1987)

[29] R. Léguillon, K. Nishio, K. Hirose, H. Makii, I. Nishinaka, R. Orlandi, K. Tsukada, J. Smallcombe, S. Chiba, Y. Aritomo et al., Physics Letters B **761**, 125 (2016)

[30] P. Möller, A. Sierk, T. Ichikawa, H. Sagawa, Atomic Data and Nuclear Data Tables **109–110**, 1–204 (2016)

[31] N. Vassh, M.R. Mumpower, G.C. McLaughlin, T.M. Sprouse, R. Surman, ApJ**896**, 28 (2020)

[32] T.M. Sprouse, M.R. Mumpower, R. Surman, Phys. Rev. C**104**, 015803 (2021)

[33] S. Rosswog, O. Korobkin, A. Arcones, F.K. Thielemann, T. Piran, MNRAS**439**, 744 (2014)

[34] B. Côté, M. Eichler, A. Yagüe López, N. Vassh, M.R. Mumpower, B. Világos, B. Soós, A. Arcones, T.M. Sprouse, R. Surman et al., Science **371**, 945 (2021)

[35] I.U. Roederer, N. Vassh, E.M. Holmbeck, M.R. Mumpower, R. Surman, J.J. Cowan, T.C. Beers, R. Ezzeddine, A. Frebel, T.T. Hansen et al., Science

**382**, 1177 (2023)

[36] O. Korobkin, A.M. Hungerford, C.L. Fryer, M.R. Mumpower, G.W. Misch, T.M. Sprouse, J. Lippuner, R. Surman, A.J. Couture, P.F. Bloser et al., ApJ**889**, 168 (2020)

[37] N. Vassh, X. Wang, M. Larivière, T. Sprouse, M.R. Mumpower, R. Surman, Z. Liu, G.C. McLaughlin, P. Denissenkov, F. Herwig, Phys. Rev. Lett.**132**, 052701 (2024)

[38] X. Wang, N. Vassh, T. Sprouse, M. Mumpower, R. Vogt, J. Randrup, R. Surman, ApJ**903**, L3 (2020)